Response to Referee #1

General Comments: The manuscript provides valuable insights into surface ozone trends in China, driven by emissions and meteorological factors, using the Fixed Emission Approximation (FEA) method. While the study is important, several key issues require attention before it can be accepted.

Response: We sincerely thank the reviewer for the positive and constructive comments on our manuscript. These suggestions have been very helpful in improving the quality and clarity of our work. We have carefully revised the manuscript accordingly.

1. The explanation of emission surrogates and the impact of coarse-resolution meteorological data on the regression process is insufficient. Additionally, regional ozone trends, especially in the PRD, need clearer explanations, and the manuscript should include maps or time-series for key ozone precursors (CO, NO_x, VOCs).

Response: Thank you for these important and constructive comments. We have addressed each point in the revised manuscript; a concise summary of our changes and rationale follows.

(1) We expanded the method section to clarify that the time variables (hour of day, month of year) serve as emission surrogates that capture regular diurnal and seasonal patterns in anthropogenic activity (e.g., traffic emission cycles). This approach is widely used in weather-normalization and RF-based attribution studies because it helps separate short-term cyclical emission variability from long-term trends (such as Grange et al., Vu et al., and Shi et al.). We also note that inclusion of these surrogates improved model performance in cross-validation. The detailed modification can be found in the revised manuscript on page 7 lines 140-143 and page 9 lines 197-198.

(2) We now explicitly state our handling of meteorological inputs: meteorological predictors were taken from the nearest ERA5 grid cell (0.25°×0.25°) to each city region, while the surface air pollutant concentrations represent multi-site city averages (i.e., averages over all available monitoring stations within each city). This city-average / nearest-grid strategy follows common practice in recent machine-learning air-quality studies and balances spatial representativeness with data availability. We have added the discussion of the limitations introduced by using coarse reanalysis fields and how this uncertainty was partially mitigated by (i) training models per city, (ii) using many meteorological predictors at multiple levels, and (iii) performing interannual resampling uncertainty tests (see new text and Fig. 2 now highlighted in the main text). We also discuss for future coupled machine learning and chemical transport modeling work to more fully assess resolution sensitivities. The detailed modification can be found in the revised manuscript on page 7 lines 144-149 and pages 22-23 lines 521-525.

(3) We expanded the results and discussion to better explain why PRD trends differ from northern regions. Key points added: (i)PRD has relatively stronger biogenic VOC and marine influences and lower anthropogenic NO_x compared with northern basins (e.g., BTH), leading to a more NO_x-limited photochemical regime; (ii) subtropical maritime climate, higher humidity and cloudiness, and frequent typhoon/monsoon perturbations modulate transport and photolysis, reducing the straightforward response of ozone to local emission changes; (iii) therefore, PRD shows smaller ozone increases in response to the same emission changes that produced larger effects in VOC-sensitive northern regions. During phase II, the trends obtained using the FEA method were generally consistent with those from previous studies using statistical methods. In this phase, the changes in ozone production sensitivity regimes in the PRD region were more pronounced compared to those in the YRD and SCB regions. We cite recent regional studies that support these mechanisms. The detailed modification can be found in the revised manuscript on page15 line 340-342 and page17 lines 387-390.

(4) We agree that precursor maps/timeseries strengthen the attribution. Accordingly, we added: (i) spatial maps of surface CO and NO_2 (ground-based where available) and column NO_2 and HCHO from TROPOMI (new Fig. 3); (ii) city-level summertime and whole year time series for CO, NO_2, and $PM_{2.5}$ for the five major regions (new Fig. S5); and (iii) discussion linking these precursor trends to regime shifts ($HCHO/NO_2$) and the FEA results (Fig. 6). Because continuous ground-based VOC observations are sparse nationally, we did not add nationwide VOC maps, instead we use satellite HCHO as an established proxy for VOC emissions. The detailed modification can be found in the revised manuscript on page12 lines 277-292, page15 lines 342-343 and page15 lines 355-356.

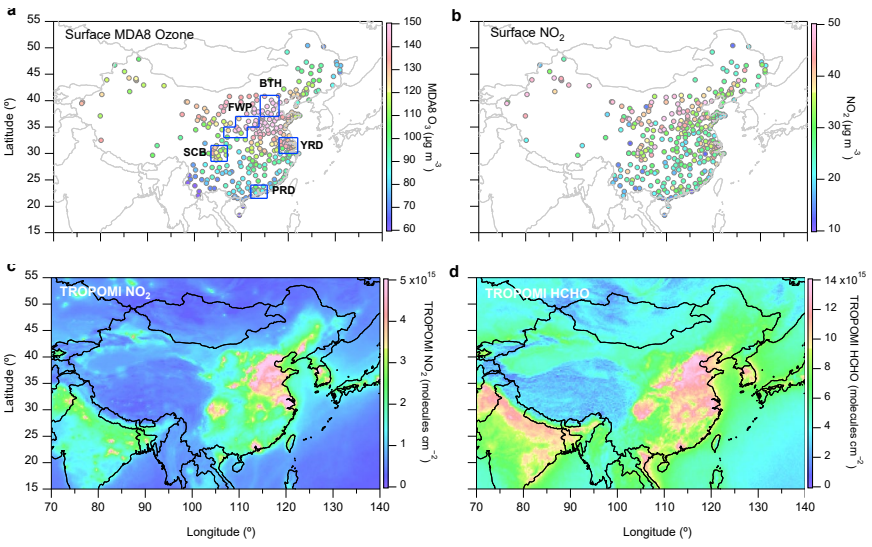

Figure 3. Spatial distribution of summertime MDA8 ozone, surface NO_2, and TROPOMI NO_2, HCHO across major city clusters in China. The panels represent the average MDA8 ozone, surface NO_2, and TROPOMI NO_2, HCHO column concentrations for 354 cities in China during the summertime (June–August) from 2018 to 2023. The corresponding five regions includes BTH (37°–41°N, 114°–118°E); YRD (30°–33°N, 118.2°–122°E); SCB (28.5°–31.5°N, 103.5°–107°E); PRD (21.5°–24°N, 112°–115.5°E) and FWP (106.25–111.25°E, 33–35°N, and 108.75–113.75°E, 35–37°N).

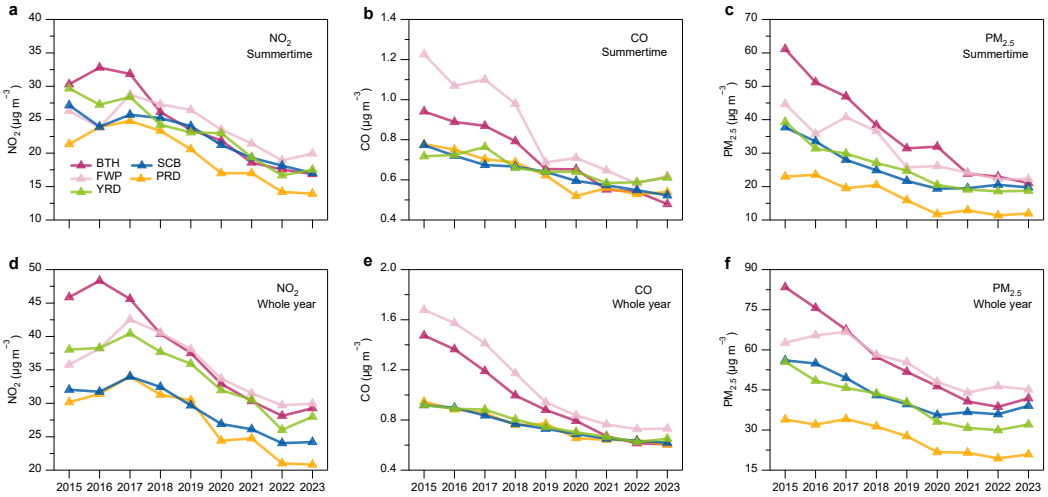

Figure S5. Ground-based observed time series of NO_2, CO and $PM_{2.5}$. Panels (a-c) show the summertime average time series of NO_2, CO, and $PM_{2.5}$ for China's five major city clusters from 2015 to 2023. Panels (e-f) present the annual average time series of NO_2, CO, and $PM_{2.5}$ for China's five major city clusters from 2015 to 2023.

2. The discussion on the COVID-19 lockdown requires more detailed analysis of TROPOMI data to explain regional ozone changes, and maps for regions like the North China Plain would help clarify spatial patterns. Figures, particularly Figure 3, lack clear quantitative results, and Section 3.3 requires deeper analysis.

Response: We sincerely thank the reviewer for these valuable and constructive comments. We have substantially revised the relevant sections to strengthen the discussion and quantitative analysis related to the COVID-19 lockdown period, as summarized below:

(1) We applied the formaldehyde-to-NO_2 ratio (FNR) diagnostic to classify ozone formation regimes and evaluate their spatial changes during the lockdown. The new analysis reveals clear regional differences: the North China Plain (NCP) and Yangtze River Delta (YRD) shifted toward more VOC-limited conditions due to sharp NO_x reductions, while parts of southern China remained in NO_x-limited or transition regimes. The updated manuscript includes corresponding maps to illustrate these spatial patterns (Fig. S13).

(2) We have significantly revised Figure 6 to provide year-round quantitative results, distinguishing the relative contributions of the three ozone sensitivity regimes (NO_x-limited, VOC-limited, and transition) over time.

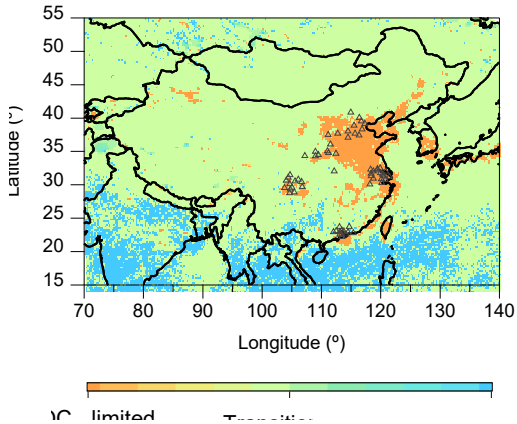

Figure S13. Ozone formation sensitivity regimes during COVID-19. Spatial distribution of ozone formation sensitivity regimes in China from January to April 2020 during the COVID-19 pandemic. The hollow triangles represent the geographical coordinates of five key urban clusters in China.

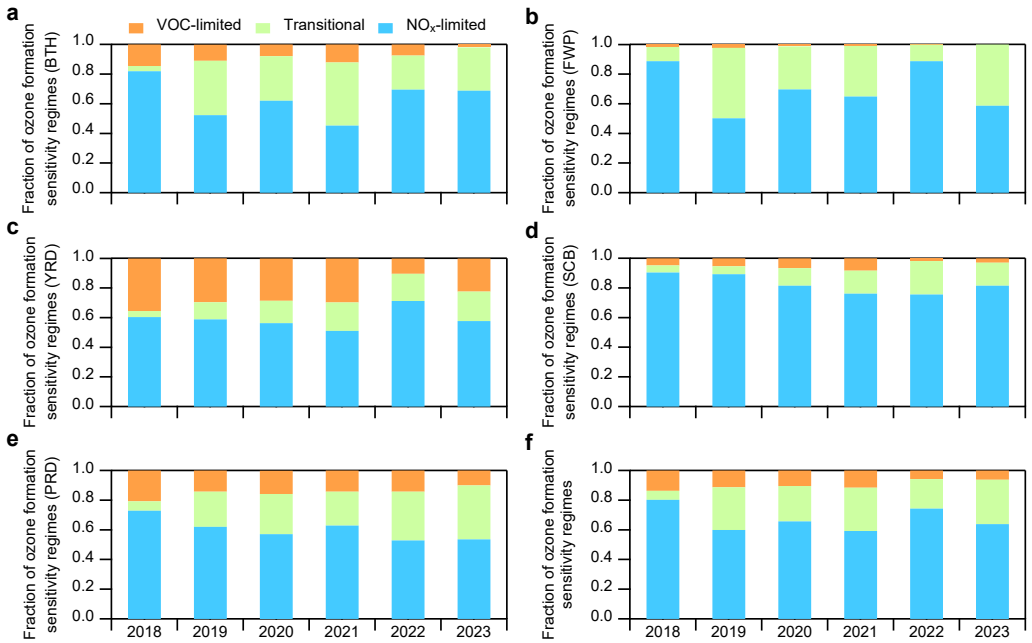

Figure 6. Trends in the distributions of ozone production sensitivity regimes. Fractions of VOC-limited, NO_x-limited, and transitional ozone sensitivity regimes across five key regions during the summertime (June to August) from 2018 to 2023, based on the FNR analysis. Panel (f) presents the overall trends for all five regions.

3. Finally, the roles of temperature, humidity, and radiation in ozone formation need clearer interpretation.

Response: We appreciate this important and constructive comment. In response, we have expanded our analysis and discussion to clarify the distinct roles of temperature, humidity, and solar radiation in ozone formation across different regions. Our extended machine learning analysis (see Fig. S16) reveals region-specific sensitivities of ozone to these meteorological factors. We also incorporated relevant literature to further support the interpretation of these regional contrasts. The detailed

modification can be found in the revised manuscript on pages 18-19 lines 430-442.

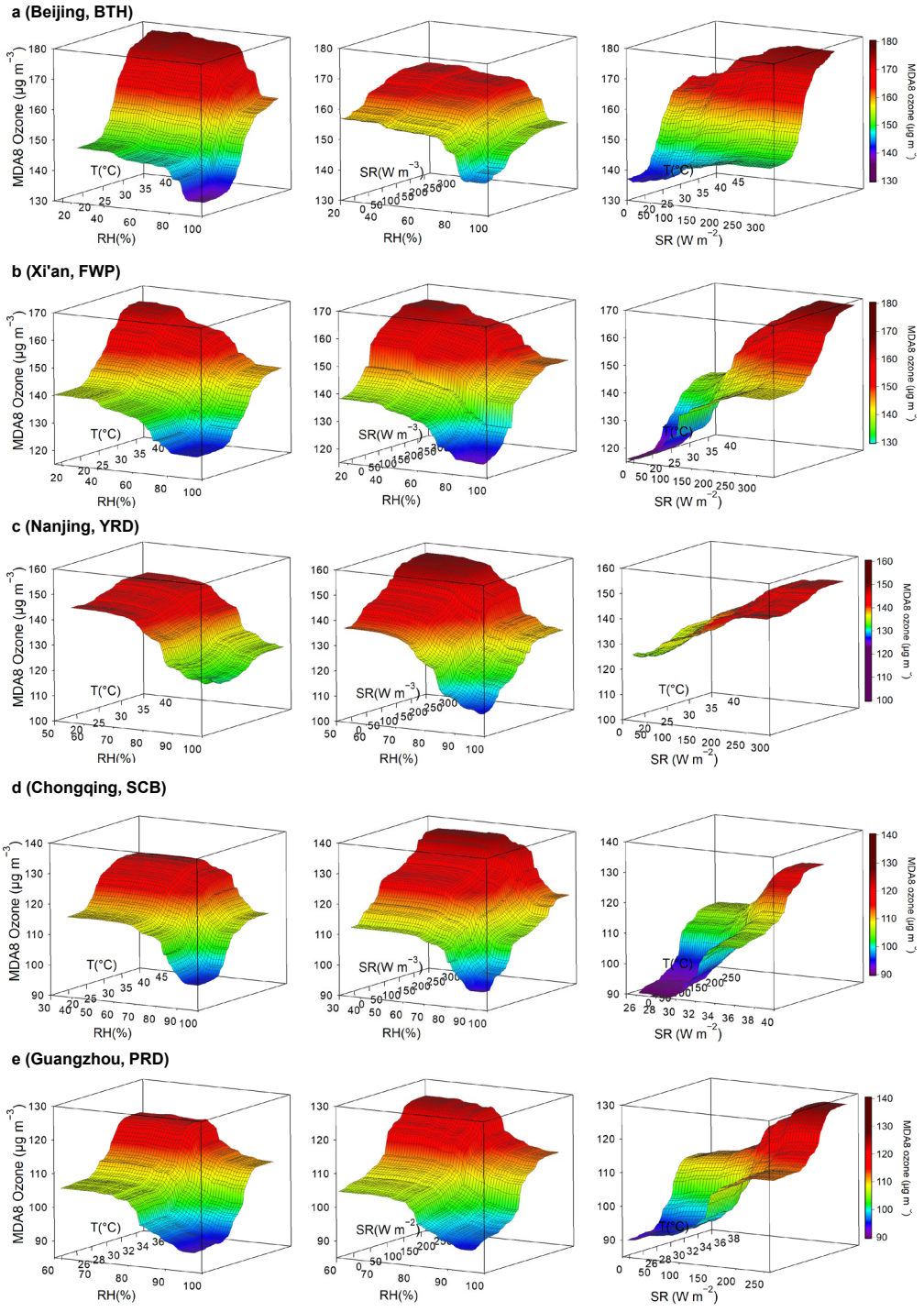

Figure S16. Partial dependence of ozone on T, RH, and SR for representative cities. Panels show the 3D-dependence plots of MDA8 ozone with RH, T, and SR for representative cities in BTH, FWP, YRD, and PRD, including MDA8 ozone-RH-T, MDA8 ozone-RH-SR, and MDA8 ozone-SR-T.

In conclusion, a major revision is needed to address these issues, strengthen the analysis, and improve the clarity and presentation of the results.

Response: We sincerely thank the reviewer for the constructive and insightful comments. We have

carefully revised the manuscript to address all the concerns raised and substantially improved the analysis, clarity, and presentation of the results. Detailed point-by-point responses and corresponding revisions are provided below.

Specific Comments:

Line 193: What is TAP?

Response: Thank you for your comment. We have clarified the meaning of TAP in the revised manuscript:

For 2013 – 2014, the surface MDA8 ozone data were obtained from the Tracking Air Pollution in China (TAP) dataset (Geng et al., 2021), which can be downloaded from http://tapdata.org (last accessed: May 20, 2024).

Line 114: How does the author account for the uncertainty in coarse-resolution meteorological variables and site data during the RF regression process? Is the specified elevation referring to the site elevation or the average elevation of the coarse-resolution meteorological variable grid?

Response: Thank you for your comment. We now explicitly state our handling of meteorological inputs: meteorological predictors were taken from the nearest ERA5 grid cell (0.25°×0.25°) to each city region, while the surface air pollutant concentrations represent multi-site city averages (i.e., averages over all available monitoring stations within each city). This city-average / nearest-grid strategy follows common practice in recent machine-learning air-quality studies and balances spatial representativeness with data availability. We compared the observed meteorological data from weather stations in Nanjing, Suzhou, and Xuzhou with the ERA5 data we used and tested the sensitivity of ozone to different meteorological datasets. We found that the parameters from ERA5 closely aligned with those from the weather stations. Sensitivity tests using different meteorological datasets showed that the predicted ozone trends under fixed 2019 emission conditions were generally consistent. This supports the reliability of ERA5 data, which, compared to weather station observations, provides a more comprehensive dataset, therefore, we chose ERA5 data for our machine learning simulations. The following compares the hourly temperature, pressure, and relative humidity observed at weather stations in Nanjing, Suzhou, and Xuzhou in 2019 with the corresponding ERA5 data for these three parameters. Additionally, we replaced these three parameters with the observed data during model training and assessed the sensitivity of ozone to different meteorological datasets:

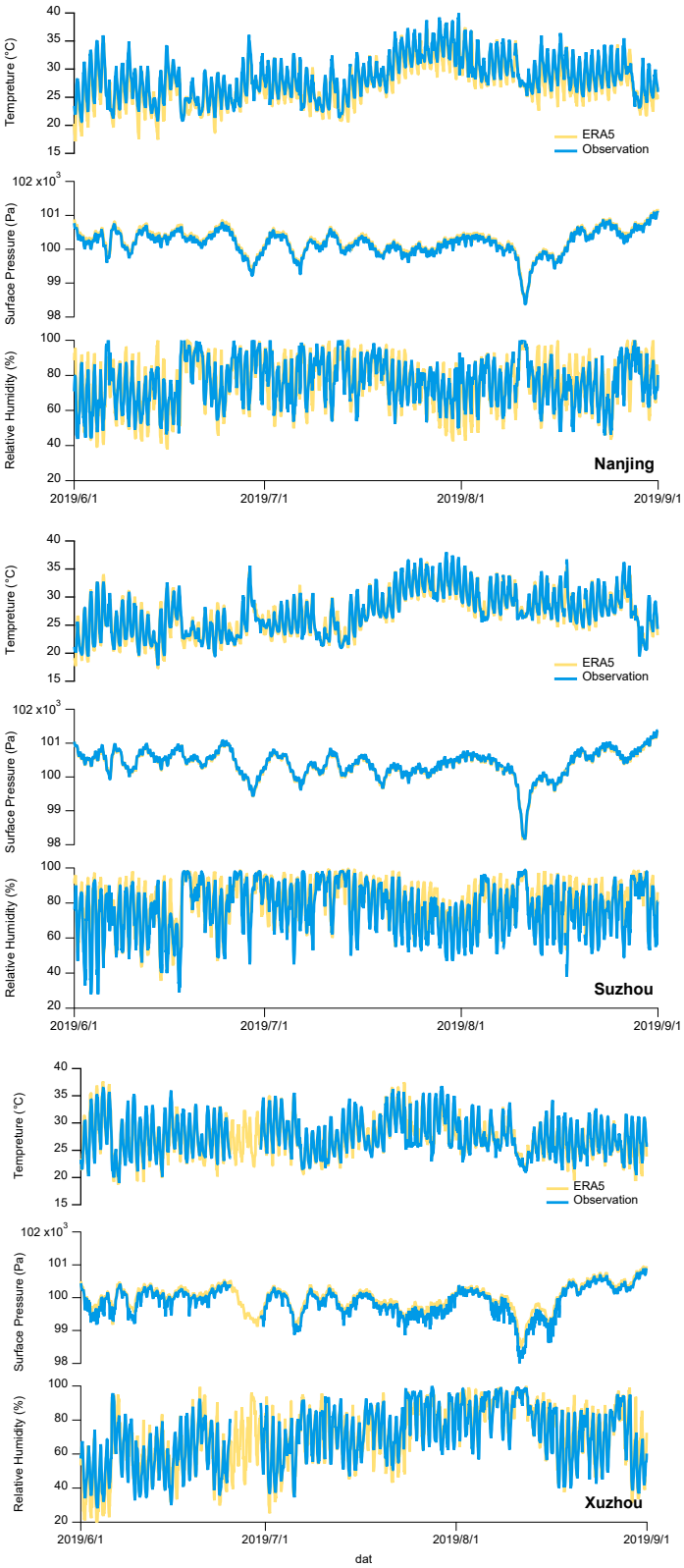
Tempreture (°C)
ERA5
Observation
102 x10^3
Surface Pressure (Pa)
Relative Humidity (%)
Nanjing
Suzhou
Xuzhou
2019/6/1
2019/7/1
2019/8/1
2019/9/1
dat

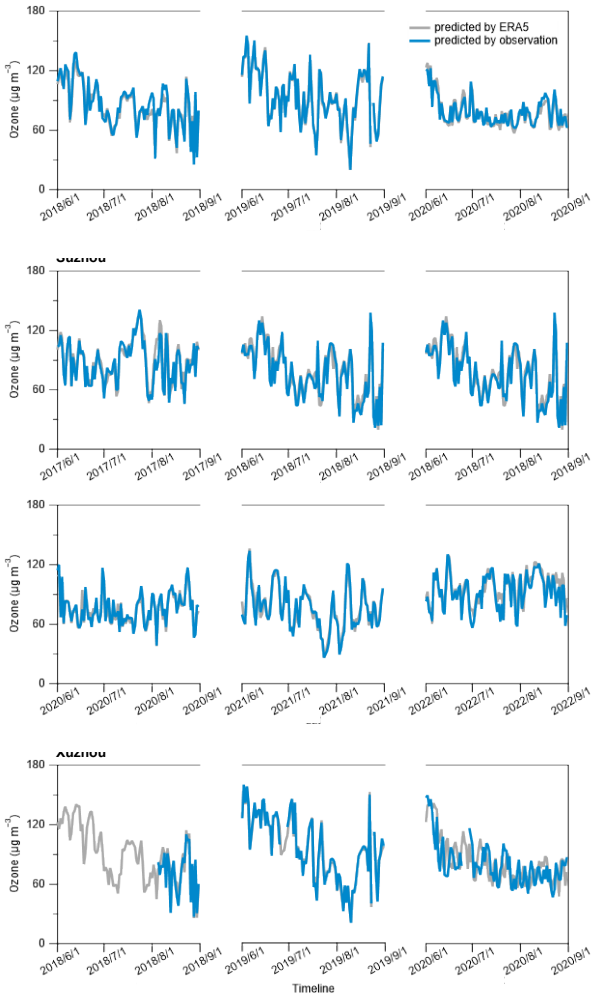

Additionally, we have added a discussion in the main text regarding the limitations introduced by using coarse reanalysis fields and how this uncertainty was partially mitigated by (i) training models for each city, (ii) using a wide range of meteorological predictors at multiple levels, and (iii) performing interannual resampling uncertainty tests. We also discuss the potential for future work that couples machine learning and chemical transport modeling to more fully assess the sensitivities to spatial resolution. The revised text now reads as follows:

It should be noteworthy that surface air pollutant observations for each city represent multi-site averages rather than data from a single monitoring station, which reduces the influence of local representativeness errors. The meteorological data are obtained from the nearest grid cell corresponding to each city, ensuring spatial consistency between the pollutant and meteorological datasets. This approach was similar to the methodologies widely adopted in previous studies (Shi et al., 2021; Wang et al., 2025; Yao et al., 2024; Zheng et al., 2023). Our modeling strategy involves building and predicting models for individual cities and for each year from 2015 to 2023, which helps in minimizing the uncertainty caused by surface heterogeneity.

Nonetheless, some limitations remain. The current implementation did not explicitly resolve

grid-scale spatial heterogeneity, vegetation, or land-use dynamics, which may influence ozone formation. Moreover, potential sensitivities to spatial resolution warrant further investigation through coupled applications of machine learning and chemical transport models.

Line 115: What is an emission surrogate? Where did the author obtain it? It should be mentioned in Section 2.1.

Response: Thank you for this helpful comment. We have expanded Section 2.1 to clarify the meaning and source of the emission surrogates. Specifically, the time variables – hour of day and month of year – are used as emission surrogates to capture regular diurnal and seasonal variations in anthropogenic activity (e.g., traffic emissions). This approach is widely applied in weather-normalization and RF-based attribution studies (e.g., Grange et al., 2018; Vu et al., 2019) to separate short-term cyclical emission variability from long-term trends. We also found that including these surrogates improved model performance during cross-validation. The revised text now reads as follows:

The time variables – hour (hour of day) and month (month of year) – are used as emission surrogates to capture regular diurnal and seasonal variations in anthropogenic activity. A similar strategy is widely applied in previous studies about long-term trends in air pollutants (e.g., Grange et al., 2018; Vu et al., 2019) to separate short-term cyclical emission variability from long-term trends.

To assess uncertainty stemming from interannual model training variability, we applied a matrix-based resampling approach (see Text S2). As shown in Fig. 2, the relative difference in residuals ranged from -9% to 3%, and remained within ±12% for all regions – supporting the robustness of the FEA method. We found that the model with the added time variables exhibited significantly smaller uncertainty compared to the model without it (Fig. S3).

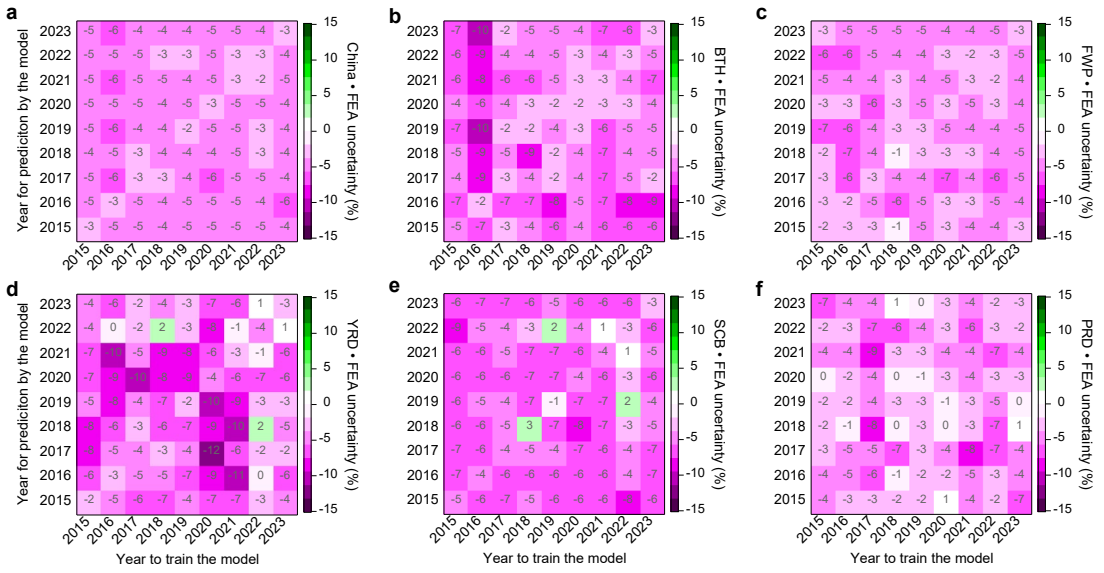

Figure 2. Uncertainty assessment of the FEA method. *The uncertainty for the FEA method is calculated using the approach described in Text S2. The diagonal line in each sub-panel represents the changes in the residuals of the models.*

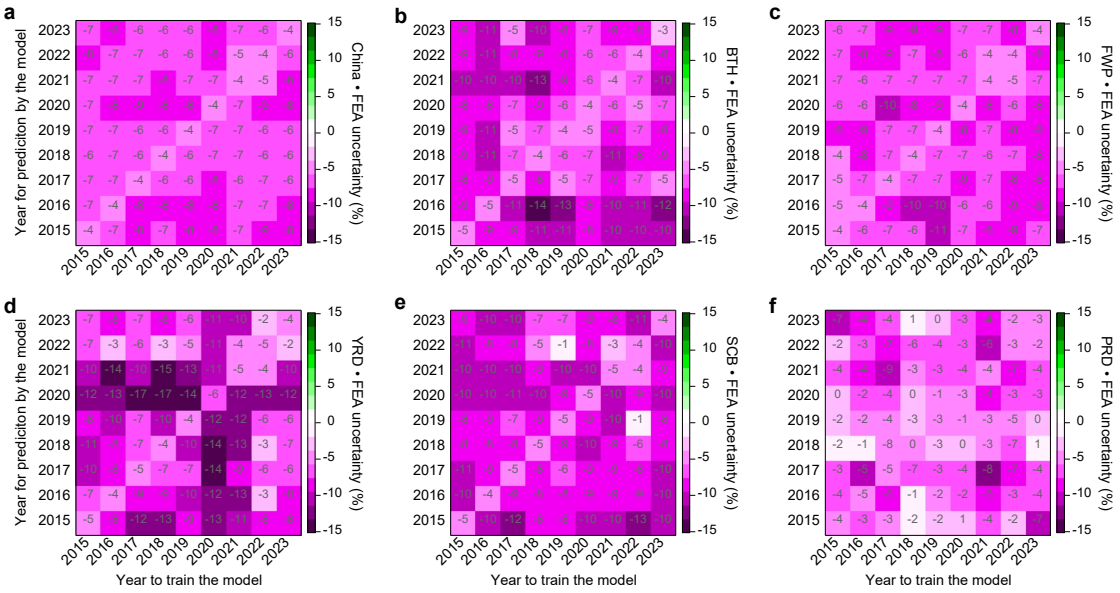

Figure S3. Uncertainty of the FEA method without time variables. *The uncertainty for the FEA method is calculated using the approach described in Text S2. The diagonal line in each sub-panel represents the changes in the residuals of the models.*

Line 117: "The aforementioned variables": It's not clear.

Response: Thank you for your comment. We have clarified the reference to "the aforementioned variables" in the revised manuscript:

First, a regression model is constructed using the random forest (RF) algorithm to relate ozone concentrations to temporal emission surrogates and to meteorological parameters at multiple atmospheric levels. These temporal emission surrogates, including month and hour, represent short-term regular emission patterns (e.g., diurnal cycles), thereby enabling the model to isolate the long-term emission-driven component of ozone changes (Grange et al., 2018; Meng et al., 2025; Shi et al., 2021; Vu et al., 2019). The meteorological parameters include 18 distinct variables at different altitudes (see Table S1).

Line 127-129: Rewrite this sentence.

Response: Thank you for your comment. We have rewritten the sentence for clarity:

Specifically, we establish hourly-resolution models for the baseline year (i) during the summer

season (June to August) as a reference for anthropogenic emissions, represented by the pink solid line in Fig. 1.

Line 243: "Anthropogenic drivers" to "Anthropogenic emission drivers".

Response: Thank you for your suggestion. We have updated it.

Line 243: You should show the anthropogenic emission map or time-series line for major ozone precursor such as CO, NO_x, and VOC.

Response: Thank you for your suggestion. We have added Ground-based observed time series of NO_2, CO and $PM_{2.5}$. The related modification is shown as follows:

As shown in Fig. S5, the precursor gases NO_2 and CO exhibited regionally distinct decreasing trends, partially explaining the spatial heterogeneity of ozone changes.

In the post-pandemic period (2020–2023), concentrations of NO_2, CO, and $PM_{2.5}$ stabilized or declined more gradually (Fig. S5), and the contribution of anthropogenic emissions to ozone variability weakened considerably (Fig. S8).

Supplement:

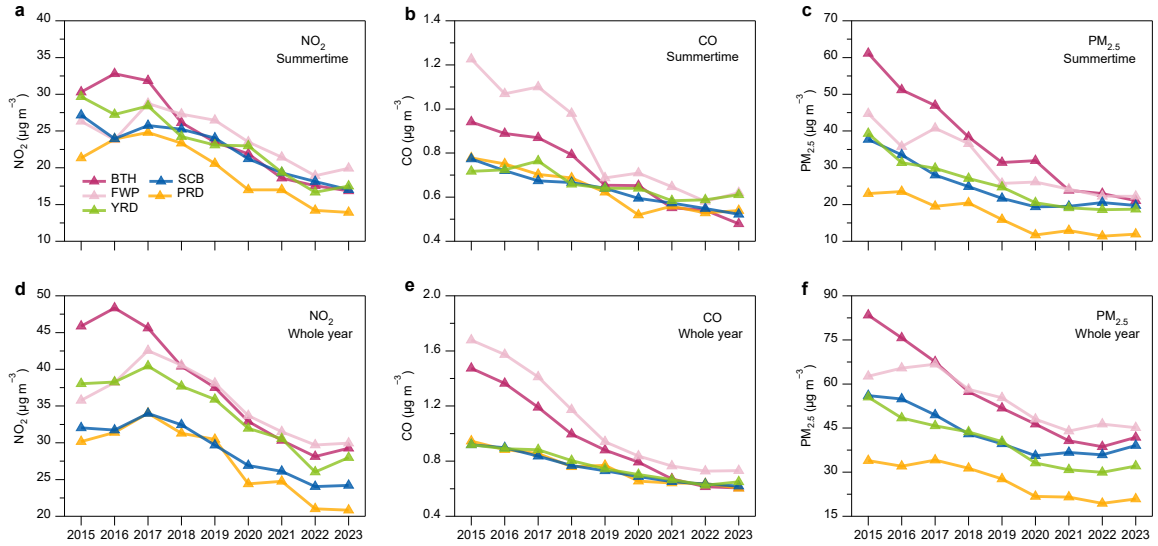

Figure S5. Ground-based observed time series of NO_2, CO and $PM_{2.5}$. *Panels (a-c) show the summertime average time series of NO_2, CO, and $PM_{2.5}$ for China's five major city clusters from 2015 to 2023. Panels (e-f) present the annual average time series of NO_2, CO, and $PM_{2.5}$ for China's five major city clusters from 2015 to 2023.*

Line 249-251: The author needs to explain why the PRD is rising and why it is falling in other regions.

Response: Thank you for your suggestion. We have added a more detailed explanation, the related

modification is shown as follows:

The most pronounced increases occurred in the FWP and BTH (45.0 ± 2.0 μg m^{-3} and 42.1 ± 2.0 μg m^{-3}, respectively), whereas the PRD exhibited a relatively modest enhancement (13.4 ± 1.6 μg m^{-3}), reflecting its predominantly NO_x-limited photochemical regime versus VOC-limited regimes in other regions (Ren et al., 2022).

Line 260: Authors should show a map to tell reader where is northern China?

Response: Thank you for your suggestion. The reference to "northern China" specifically pertains to the BTH (Beijing-Tianjin-Hebei) and FWP (Fenwei Plain) city clusters in northern China. We have now clarified this in the manuscript.

Line 260-262: Prior to 2017, PRD consistently recorded the lowest ozone concentrations among these major regions. Intuitively, the PRD appears to have the least potential for ozone reduction. Yet why did both the YRD and SCB regions exhibit smaller reduction margins than the PRD?

Response: Thank you for your comment. During phase II, MDA8 ozone decreased by 10.5 ± 2.0 μg m^{-3} in BTH and 10.4 ± 3.0 μg m^{-3} in FWP, with smaller declines in YRD (–4.8 ± 3.8 μg m^{-3}), SCB (–2.8 ± 2.4 μg m^{-3}), and PRD (–6.6 ± 1.4 μg m^{-3}). These changes are attributed to anthropogenic emission controls. Our results are generally consistent with those obtained by Wang et al. (2023) using statistical methods. Notably, the PRD region showed relatively larger changes compared to YRD and SCB, which can be attributed to shifts in the ozone production sensitivity regimes. We have provided a detailed explanation of these changes in the main text:

The SCB region consistently exhibited strong NO_x limitation (>75%), whereas the PRD showed a gradual expansion of the transitional regime alongside a modest contraction of VOC-limited areas. These shifts in photochemical sensitivity correspond well with the ozone decrease observed during Phase II emission reductions.

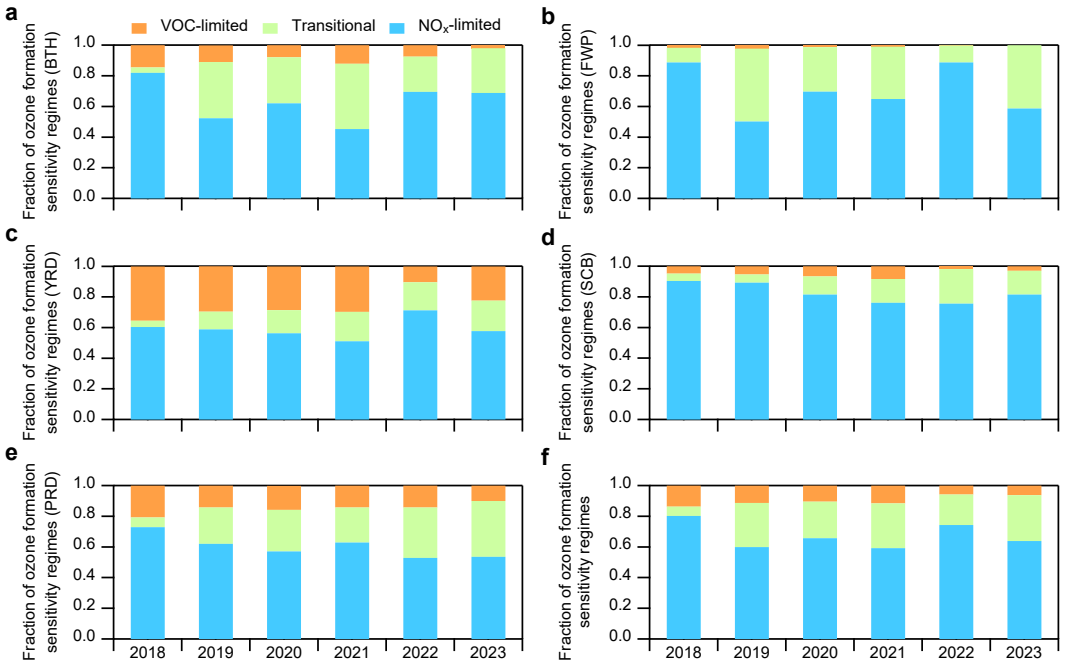

Figure 6. Trends in the distributions of ozone production sensitivity regimes. *Fractions of VOC-limited, NO_x-limited, and transitional ozone sensitivity regimes across five key regions during the summertime (June to August) from 2018 to 2023, based on the FNR analysis. Panel (f) presents the overall trends for all five regions.*

Line 266-268: The author should inform readers: How much have anthropogenic emissions decreased in major regions due to the nationwide lockdown?

Response: Thank you for your suggestion. We have added quantitative information on emission reductions during the nationwide lockdown. The revised text reads:

The COVID-19 pandemic (January-April 2020) introduced an unprecedented perturbation to anthropogenic activity, leading to sharp declines in industrial production, energy consumption, and transportation (Shi and Brasseur, 2020; Zheng et al., 2021). National emissions of SO_2, NO_x, $PM_{2.5}$, and VOCs were estimated to have decreased by 0.37 Tg (12%), 0.87 Tg (13%), 0.25 Tg (10%), and 1.07 Tg (12%), respectively, relative to the same period in 2019 (Geng et al., 2024).

Line 273-275: The author suggests that the rise in ozone concentrations is due to suppressed NO titration. Therefore, the author could fully utilize TROPOMI data to analyze changes in sensitive zones during the COVID-19 period. This may help explain why ozone concentrations in the remaining 20% of cities decreased during the COVID-19 pandemic.

Response: Thank you for your suggestion. We applied the formaldehyde-to-NO_2 ratio (FNR)

diagnostic to classify ozone formation regimes and evaluate their spatial changes during the lockdown. The new analysis reveals clear regional differences: the North China Plain (NCP) and Yangtze River Delta (YRD) shifted toward more VOC-limited conditions due to sharp NO_x reductions, while parts of southern China remained in NO_x-limited or transition regimes. The updated manuscript includes corresponding maps to illustrate these spatial patterns (Fig. S13). the related modification is shown as follows:

Spatial distributions of ozone formation sensitivity during the COVID-19 lockdown (Fig. S13) reveal that most of China was in a transitional regime, with major urban clusters remaining VOC-limited and only limited areas in southern China being NO_x-limited. This spatial pattern aligns with the observed widespread ozone increases during the lockdown (Fig. S7).

Supplement:

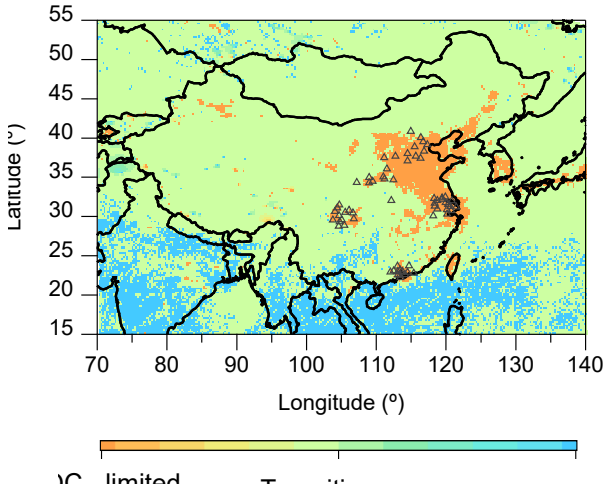

Figure S13. Ozone formation sensitivity regimes during COVID-19. *Spatial distribution of ozone formation sensitivity regimes in China from January to April 2020 during the COVID-19 pandemic. The hollow triangles represent the geographical coordinates of five key urban clusters in China.*

Line 275-276: The author should explain how anthropogenic emissions have changed during this period.

Response: Thank you for your suggestion. We have added Ground-based observed time series of NO_2, CO and $PM_{2.5}$, which provide insights into the changes in anthropogenic emissions during this period. The related modification is shown as follows:

In the post-pandemic period (2020–2023), concentrations of NO_2, CO, and $PM_{2.5}$ stabilized or declined more gradually (Fig. S5), and the contribution of anthropogenic emissions to ozone variability weakened considerably (Fig. S8).

Supplement:

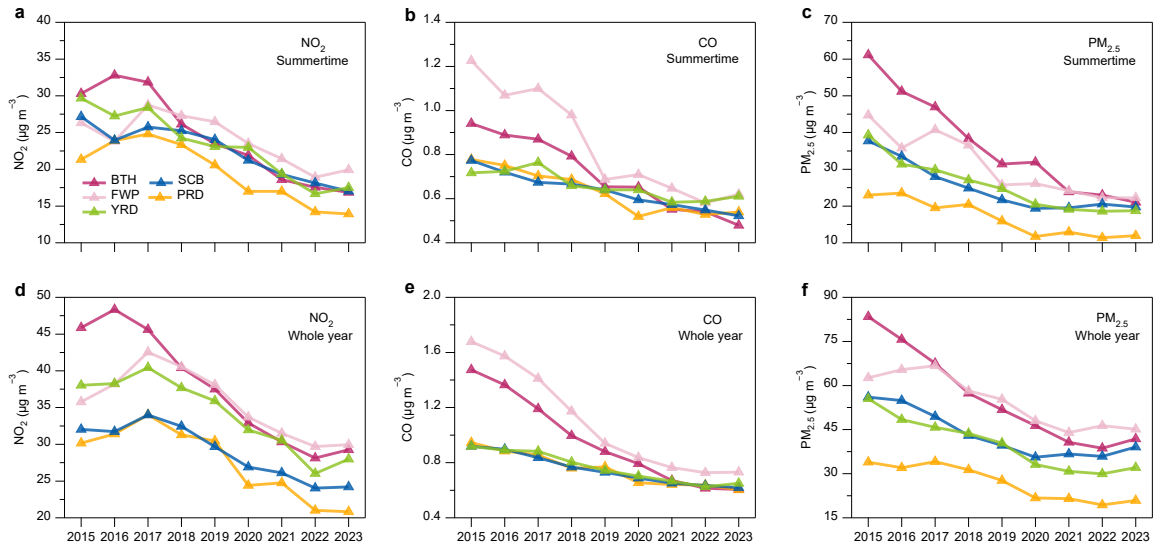

Figure S5. Ground-based observed time series of NO_2, CO and $PM_{2.5}$. *Panels (a-c) show the summertime average time series of NO_2, CO, and $PM_{2.5}$ for China's five major city clusters from 2015 to 2023. Panels (e-f) present the annual average time series of NO_2, CO, and $PM_{2.5}$ for China's five major city clusters from 2015 to 2023.*

Line 295: Where is North China Plain?

Response: Thank you for your comment. We have marked the coordinates of the North China Plain (NCP) on the map. The related modification is shown as follows:

Supplement:

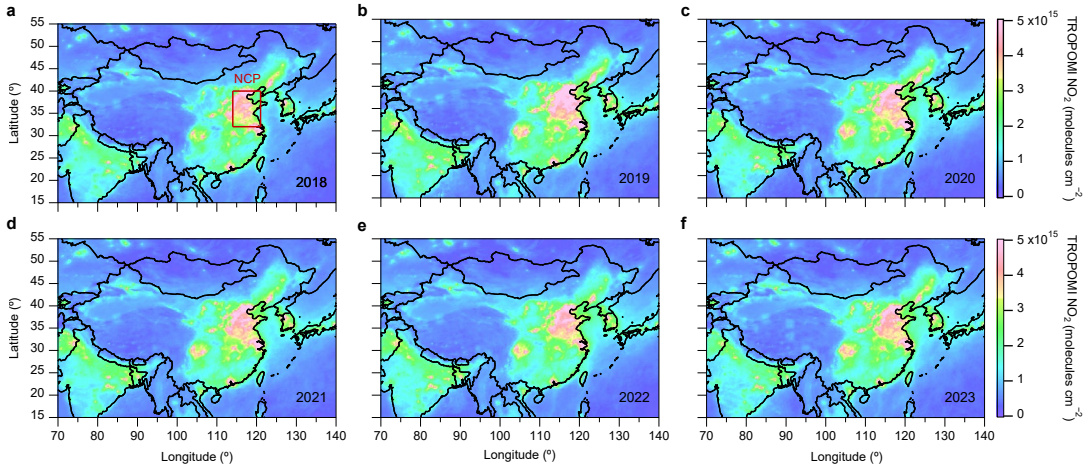

Figure S10. Spatial and temporal variations of satellite NO_2. *Map of average levels of satellite-observed NO_2 from June-August 2018 to 2023. The rectangle in panel (a) represents the extent of the North China Plain (NCP).*

Line 297: "The Yangtze River Delta" to "YRD".?

Response: Thank you for your suggestion. We have corrected the error.

Line 298-299: You can show a Δtemperature map from ERA5 data.

Response: Thank you for your suggestion. We have added a spatial distribution of daytime temperature differences between HW and NHW. The related modification is shown as follows:

Between 2018 and 2023, NO_2 columns over the North China Plain (NCP) declined from 4.13 × 10^{15} to 3.85 × 10^{15} molecules cm^{-2}, while HCHO remained stable until 2021, followed by a sharp increase in 2022. The spatial pattern of temperature anomalies between heatwave (HW) and non-heatwave (NHW) periods (Fig. S11) reveals strong positive differences in the YRD and SCB, consistent with enhanced biogenic and anthropogenic VOC emissions under extreme heat (Qin et al., 2025; Tao et al., 2024).

Supplement:

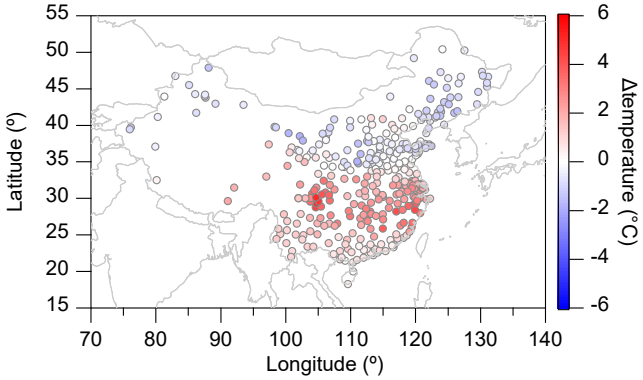

Figure S11. Spatial distribution of daytime (11:00-17:00) temperature differences between HW and NHW. *The HW period is defined as July 16 to August 31, 2022, while the corresponding period in other years is considered as NHW.*

Line 306-307: The author might use this to explain why the PRD's changes differ from those of other cities in Section 3.2.

Response: Thank you for your suggestion. We have incorporated the concept of differences in ozone sensitivity intervals in Section 3.2 to clarify why the changes in the PRD differ from those of other cities. The related modification is shown as follows:

The most pronounced increases occurred in the FWP and BTH (45.0 ± 2.0 μg m^{-3} and 42.1 ± 2.0 μg m^{-3}, respectively), whereas the PRD exhibited a relatively modest enhancement (13.4 ± 1.6 μg m^{-3}), reflecting its predominantly NO_x-limited photochemical regime versus VOC-limited regimes in other regions (Ren et al., 2022).

The SCB region consistently exhibited strong NO_x limitation (>75%), whereas the PRD showed

a gradual expansion of the transitional regime alongside a modest contraction of VOC-limited areas. These shifts in photochemical sensitivity correspond well with the ozone decrease observed during Phase II emission reductions.

Figure 3: It is recommended that the author label the locations of major regions on this map.

Response: Thank you for your suggestion. In the revised manuscript, we have replaced the corresponding image with a map showing the trend of ozone sensitivity intervals across the five major city clusters of China from 2018 to 2023. Additionally, the map in the supplementary material has also been updated to reflect the latitude and longitude range corresponding to the five major city clusters.

The related modification is shown as Fig. 6 and Fig. S12.

Section 3.3: Lack of quantitative results. Figure 3 fails to clearly show the interannual changes in sensitive areas. The authors should adopt a more explicit presentation method to highlight the differences in area among sensitive zones in each region.

Response: Thank you for your insightful comments and suggestions. We have revised Section 3.3 and enhanced the presentation of Figure to better highlight the interannual changes in sensitive areas. A more explicit method has been adopted to clearly show the differences in area among the sensitive zones in each region. The related modification is shown as follows:

To diagnose the evolving chemical sensitivity of ozone production, we examined the spatiotemporal evolution of the HCHO/NO_2 ratio (Text S1). Figure S12 shows that this ratio exhibited regionally distinct transitions from 2018 to 2023, reflecting shifts in photochemical regimes. Figure 6 summarizes the relative contributions of VOC-limited, NO_x-limited, and transitional regimes across the five key regions. In BTH, NO_x-limited areas accounted for ~82% of the domain in 2018 and remained above 45% thereafter, while VOC-limited regions declined from ~14% to ~2%. In FWP, summer ozone formation was largely controlled by NO_x-limited and transitional regimes. The YRD underwent a notable shift from VOC- to NO_x-limited chemistry, with VOC-limited fractions decreasing from ~35% in 2018 to ~22% in 2023, particularly during 2022 when extreme heat amplified VOC emissions and photochemical activity (Qin et al., 2025; Tao et al., 2024). The SCB region consistently exhibited strong NO_x limitation (>75%), whereas the PRD showed a gradual expansion of the transitional regime alongside a modest contraction of VOC-limited areas. These shifts in photochemical sensitivity correspond well with the ozone decrease observed during Phase II emission reductions.

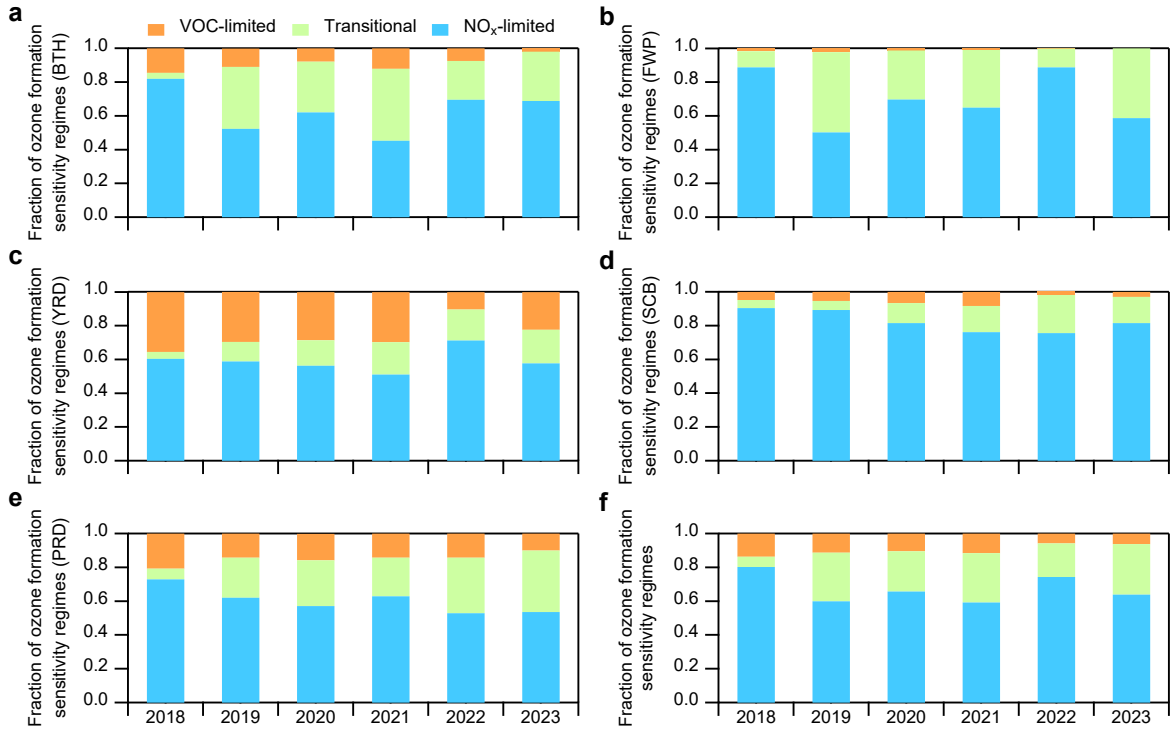

Figure 6. Trends in the distributions of ozone production sensitivity regimes. *Fractions of VOC-limited, NO_x-limited, and transitional ozone sensitivity regimes across five key regions during the summertime (June to August) from 2018 to 2023, based on the FNR analysis. Panel (f) presents the overall trends for all five regions.*

Line 337-350: Authors cannot merely provide quantitative descriptions; ACP journals require authors to conduct deeper analysis of these quantitative results.

Response: Thank you for your insightful comments and suggestions. We have revised the manuscript to provide a deeper analysis of the quantitative results presented. This includes a more detailed interpretation of the data and its implications.

The corresponding modifications can be found in Section 3.3.

Line 356-357: That's a boring sentence. Although the author provides some explanation in lines 358-359, this explanation is overly broad. For example, why are RH and temperature the dominant factors in other regions, while shortwave radiation and RH are the dominant factors in the YRD region? What is the relationship between temperature and radiation? Which variable is the fundamental cause of ozone concentration changes, and what role does RH play in this process?

Response: Thank you for your insightful comments. We have removed the sentence and we have expanded our analysis and discussion to clarify the distinct roles of temperature, humidity, and solar

radiation in ozone formation across different regions. Our extended machine learning analysis (see Fig. S16) reveals region-specific sensitivities of ozone to these meteorological factors. The related modification is shown as follows:

Partial dependence analysis (Fig. S16) further illustrates the nonlinear responses of ozone to key meteorological factors (T, RH, SR) for representative cities in each cluster, revealing clear regional contrasts. In Beijing (BTH), ozone concentrations show the strongest positive response to T (Fig. S16a), consistent with the enhancement of reaction kinetics and biogenic VOC emissions under hot conditions. This behavior reflects the thermodynamic coupling between surface heating, boundary-layer expansion, and photochemical production. In Nanjing (YRD), ozone is more sensitive to solar radiation than to temperature (Fig. S16c), highlighting the dominant role of actinic flux in controlling radical production during warm and dry conditions. Yang et al. (2024) similarly reported that high-temperature and low-RH conditions over the NCP and YRD enhance photochemical ozone formation, with chemical production being the dominant process driving ozone buildup during the most polluted months. In the SCB, both T and RH exhibit strong influences, while in the PRD, ozone variability is shaped primarily by T and large-scale circulation patterns associated with subtropical maritime flow and typhoon incursions from the Northwest Pacific (Chen et al., 2024; Wang et al., 2024a; Wang et al., 2022a).

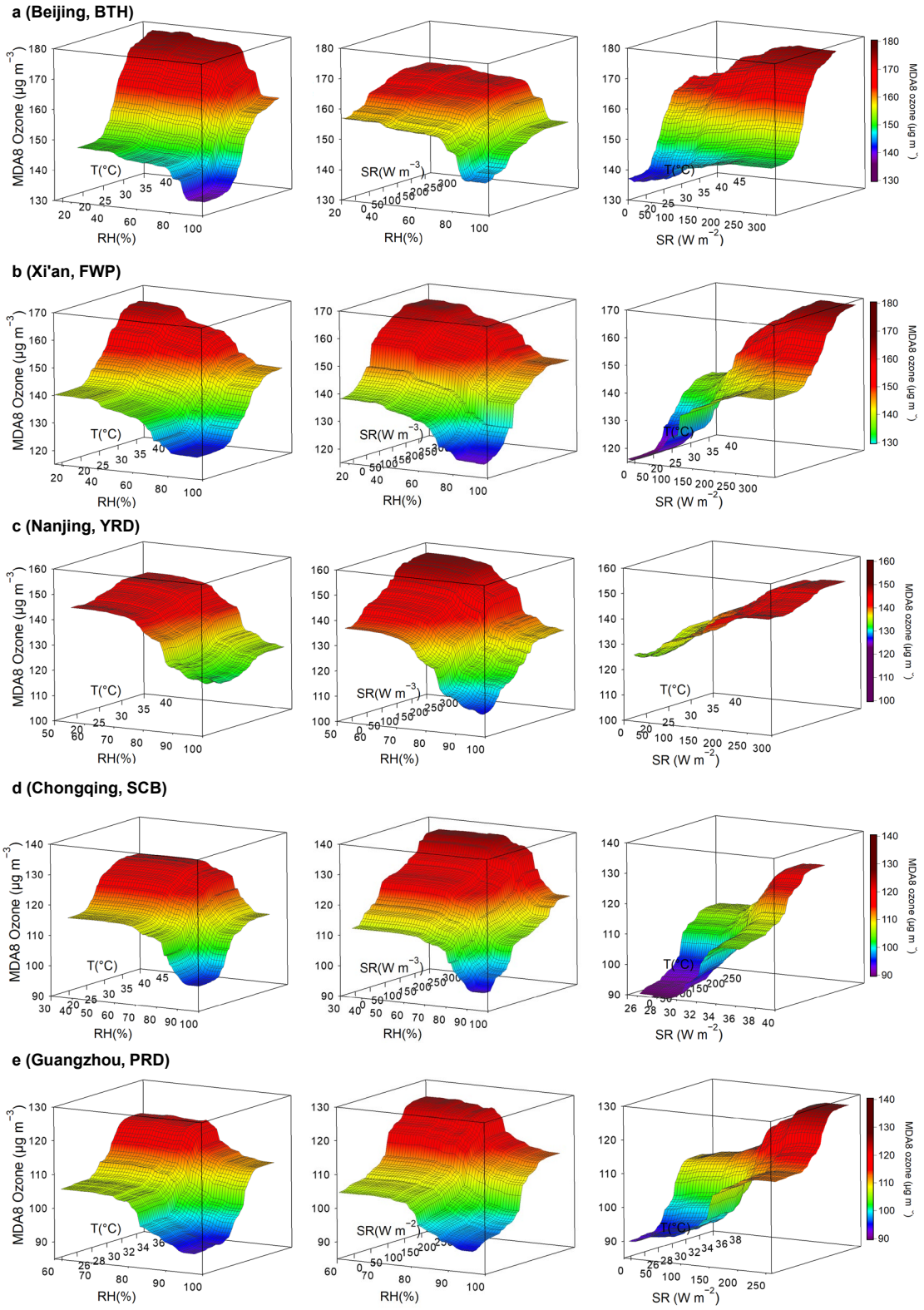

Figure S16. Partial dependence of ozone on T, RH, and SR for representative cities. *Panels show the 3D-dependence plots of MDA8 ozone with RH, T, and SR for representative cities in BTH, FWP, YRD, and PRD, including MDA8 ozone-RH-T, MDA8 ozone-RH-SR, and MDA8 ozone-SR-T.*

Line 369-371: Figure S13 shows that the correlation between T and SR in inland southern China is very low during both HW and NHW periods. Why is this? Additionally, the correlation for RH between HW and NHW appears significantly different. I recommend that the authors adjust the colorbar in Figure S13E-F to a red-blue scale with zero centered. This may reveal positive correlations for RH in certain regions.

Response: Thank you for your insightful comments and suggestions. We appreciate the reviewer pointing out the issue. The correlation does not imply causality, and Figure S13 should not have been used as evidence. We have removed the corresponding content from the manuscript.

Line 379: "amplifying" to "increasing".

Response: Thank you for your suggestion. We have replaced "amplifying" with "increasing".

Line 383-384: I do not agree that. Cloud cover directly influences temperature and shortwave radiation variations and should not be considered a secondary effect.

Response: Thank you for your suggestion, we agree with you. During extreme weather events, ozone variation is influenced by multiple meteorological parameters, and there is no primary or secondary relationship among them. We have revised the manuscript accordingly. The revised sentence is as follows:

A multi-year comparison (Fig. 7) highlights the opposing effects of key meteorological variables – including RH, T, boundary layer height (BLH), total precipitation (TP), and surface pressure (SP) – on MDA8 ozone.

Line 387: What is the RH effect?

Response: Thank you for your comment. We have modified the corresponding text to avoid ambiguity. The revised sentence is as follows:

The trend in ΔSHAP values under high-humidity conditions from 2015 to 2023 (Fig. S20) further confirms the model's ability to capture the suppressive effects of wet weather conditions on ozone formation.